Interparticle Interactions and Self-Assembly of Functionalized Nanodiamonds

ARTICLE *in* JOURNAL OF PHYSICAL CHEMISTRY LETTERS · APRIL 2012

Impact Factor: 7.46 · DOI: 10.1021/jz300066j

2 AUTHORS, INCLUDING:

Amanda S Barnard

The Commonwealth Scientific and Industrial …

181 PUBLICATIONS **4,317** CITATIONS

THE JOURNAL OF PHYSICAL CHEMISTRY Letters

Letter

pubs.acs.org/JPCL

Interparticle Interactions and Self-Assembly of Functionalized Nanodiamonds

Lin Lai and Amanda S. Barnard*

CSIRO Materials Science and Engineering, Clayton, VIC, 3168, Australia

ABSTRACT: Although unpassivated detonation nanodiamonds are known to form tightly bound (and sometimes ordered) superstructures, in most high performance applications the surface are deliberately functionalized, and this can profoundly alter the aggregation behavior. In the present study, we model the aggregation of functionalized nanodiamonds and show that functionalization greatly reduces the Coulombic interactions characteristic of unsaturated particles. Our results provide new insights into the interactions of functionalized nanoparticles.

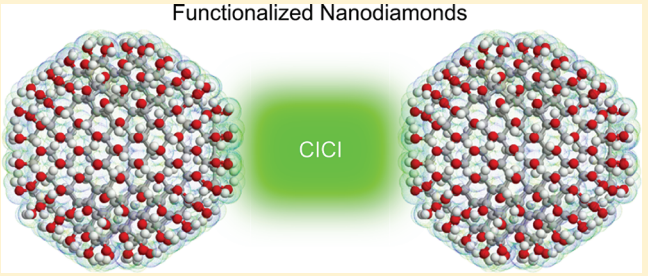

SECTION: Nanoparticles and Nanostructures

Nanodiamonds (NDs) are unique structures that have been proposed for a variety of technical applications including components for optoelectronic devices,[1] composites,[2] and new emerging applications in the field of biology and nanomedicine,[3−8] such as drug delivery[4,5] and biolabeling.[3] These applications are largely dependent on the availability of a large quantity of monodispersed single-digit diamond nanoparticles[9] and the way that these individual particles interact with each other or with other molecules. For example, Huang et al. showed that doxorubicin hydrochloride (DOX), an apoptosis-inducing drug widely used in chemotherapy, may be successfully adsorbed on the surfaces of NDs and/or embedded into the intervals of ND aggregates, and introduced into living cells. The mechanism of salt-mediated adsorption of DOX onto NDs, in aqueous solution, is contingent on the repulsive interaction of DOX−DOX and ND−ND being less than the cohesive interaction of ND−DOX, so at that a sufficient amount of DOX can be adsorbed onto the particles. It was also shown that, since the DOX resides within the aggregates due to ND−ND interactions, a protective or shielding effect was displayed, which delayed DOX desorption and facilitated a slow-release activity that could potentially prolong efficacy and reduce side effects.[10] The strength and frequency of ND interactions, which determines the aggregation behavior, is critical.

In general, NDs tend to form large tightly bound aggregates on the order of ∼100 nm in size during the cooling cycle of the detonation shock wave,[11] and the aggregates can not be dispersed using the ultrasound alone.[12] The persistent aggregation of NDs perplexed researchers for decades, and several approaches such as ball-milling,[11] graphitization/oxidation,[13] or burning in air[14] were suggested to reduce the aggregates into primary particles despite their respective drawbacks. Very recently, it was reported by Williams and coauthors[12] that hydrogenation via annealing NDs in hydrogen gas results in breakdown of ND aggregates and the recovery of the monodispersed primary nanoparticles. However, aggregation is not always undesirable, and it has also been shown that ordered superstructures (called agglutinates) may be formed through spontaneous ND self-assembly.[15] It is this different type of aggregation that has proven to be useful, providing controlled elution or extraction mechanisms during drug delivery.

The underlying mechanism for the formation of ND aggregates has been heavily debated. It was first assumed that the agglutinates were held together by random van der Waals interparticle interactions. However, this assumption was abandoned because the agglomerates strongly resisted dispersion,[9] and a large driving force is required to disintegrate ND aggregates. A reasonable explanation for this problem was offered by Barnard and Sternberg.[16] Using self-consistent charge density functional tight-binding method (SCC-DFTB), they demonstrated that the distribution of the electrostatic potential on bucky-diamonds (characterized by a diamond-like core and a graphitic outer shell) is anisotropic and facet-dependent. It was reported that on a truncated octahedral bucky-diamond, the {100} facets exhibit a strong positive electrostatic potential, while half of the {111} facets exhibit a strong negative potential. The other half was found to be charge neutral due to the difference in particle morphology and symmetry of the charge-negative type of {111} surfaces, and the incomplete graphitization of the surface. Therefore, the interparticle interaction underlying the aggregation of bucky-diamond was attributed to coherent interfacial Coulombic interactions (CICIs), upon which several different networks or superstructures may be proposed.[17] A more random aggregation based on the same mechanism is referred to as

Received: January 16, 2012
Accepted: March 10, 2012

   dx.doi.org/10.1021/jz300066j | J. Phys. Chem. Lett. 2012, 3, 896−901

incoherent interfacial Coulombic interactions (IICI). This self-assembly mechanism based on electrostatic interaction has subsequently been confirmed by high-resolution aberration corrected transmission electron microscopy (HRTEM) observations.[18,19]

However, while it is possible to obtain samples of "bare" bucky-diamonds, in practice, NDs are generally terminated with a variety of chemical groups due to the active nature of the surfaces. The possible surface terminations are found to be −COOH, −CONH, −OH, −CO, $-NH_2$, −SH, $-CH_2$, and −H.[20] Previous studies have demonstrated that under normal conditions surface-functionalized NDs are thermodynamically more favorable than the corresponding bucky-diamond under atmospheric conditions,[21,22] and it is unclear how robust the CICI and IICI mechanisms are with respect to surface passivation and functionalization. A complete examination of the interparticle interactions between functionalized NDs is essential in improving our knowledge of the aggregation of diamond nanoparticles for use under therapeutically relevant conditions, and advancing the functionalization-assisted development or porous superstructures.

Similar to previous works,[21,22] C_{705} and C_{837} NDs are chosen as model structures to examine the impact of particle morphology on the interparticle interaction. Therefore, to be directly comparable with previous work, all the calculations in this study have been performed using SCC-DFTB,[23,24] which was implemented in the DFTB+ code. This approximate quantum chemistry approach is based on a second-order expansion of the Kohn−Sham total energy in density functional theory (DFT) with respect to charge density fluctuations. The reference density is derived from self-consistent DFT calculations for the weakly confined neutral atoms, and the confinement potential is optimized to meet the charge density and effective potential in molecules and solids. Two-center tight-binding matrix elements are explicitly included using a minimal valence basis within the DFT level. A universal short-range repulsive potential accounts for double counting terms in the Coulomb and exchange-correlation contributions, as well as the internuclear repulsion, and self-consistency is included at the level of Mulliken charges.[24] This method has been successfully applied to study the structure and thermodynamical stability of NDs with and without surface functionalization.[16−18,21,22,25−27] The pbc set of parameters was used involving hydrogen, oxygen, and carbon reported by Köhler and co-workers.[28]

In each case, we fully terminated the surface dangling bonds on the surface of the C_{705} and C_{837} NDs with hydrogen atoms or hydroxyl groups, respectively, and then relaxed their structures until forces on each atom was minimized to be less than 10^{-4} a.u. (i.e., ≈ 5 meV/Å). These simulations are consistent with previous studies.[21,22] As in previous works, we deliberately excluded van der Waals contributions, as we are focusing on the Coulombic interactions, and it is essential that we know at all times where our interaction is coming from. As we will see, the interaction energy of the functionalized NDs is greater than the energy of van der Waals interactions in carbon (based on the graphite interlayer energy), but van der Waals interactions may be worth investigating in the future.

To identify the underlying mechanism in the interparticle interaction of the aggregated, functionalized diamond nanoparticles, their surface electrostatic potentials (SEPs) were calculated based on these fully relaxed structures. The SEP of the functionalized NDs are found to be quite different from that of the pristine bucky-diamonds previously reported.[16] Generally, hydrogenated nanoparticles display an almost homogeneous and slightly negative SEP (Figure 1a,b),

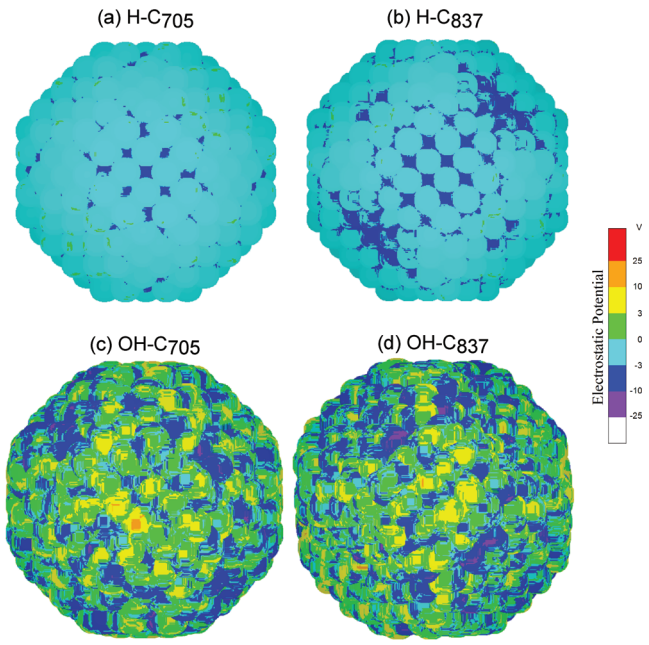

Figure 1. SEP of hydrogen- and hydroxyl-passivated C_{705} and C_{837} NDs. This potential is calculated using Coulomb's law considering the charge associated with each atom. The legend shows the static assignment of colors using a dielectric constant value of 10.[30]

especially in the hydrogenated C_{705} ND (H−C_{705}). There is a vague anisotropy in the hydrogenated C_{837} ND (H−C_{837}), where the SEP in (111) facets was a little more negative than that in the (111)* facets (Figure 1b). Here, (111)* is distinguished from (111) given the structural asymmetry described in ref 16. By contrast, hydroxylation of NDs gives rise to a more complicated distribution of the SEP in both C_{705} and C_{837} NDs (Figure 1c,d). In the hydroxylated C_{705} ND (OH−C_{705}), the {100} facets, {110} facets, (110)−(111) edges, and (100)−(110) edges display a bias toward positive potential, while the SEP on the {111} facets are largely negative. In the hydroxylated C_{837} ND (OH−C_{837}) the SEPs are largely positive on the {100} facets, largely negative on the (111) facets, and somewhat mixed on the (111)* facets. While this trend is qualitatively consistent with bucky-diamonds, the degree of facet-dependent anisotropy is significantly lower than that in the bucky-diamonds, which will have important consequences for the way these NDs interact with their surroundings[29] and each other.

To explore these consequences, we have modeled the interparticle interactions by performing a series of static total energy calculations on a pair of functionalized nanoparticles with respect to interfacial separation and interfacial rotation. Each pair of nanoparticles is aligned with the interacting surfaces parallel to each other, sharing the same normal vector. For each configuration, the particles were first fixed at a separation distance of 1.5 Å. By keeping one of them fixed and rotating the other one around the common normal vector, a series of total energies were calculated with respect to the interfacial angle. This provides a measure of interfacial coherence. Once the energetically preferred angle was determined, it was fixed, and another series of static total

dx.doi.org/10.1021/jz300066j | J. Phys. Chem. Lett. 2012, 3, 896−901

energy calculations was performed with varying separation distances to determine the equilibrium separation distances. In all cases, the separation distance is defined as the nearest distance (normal to the facets considered) between functional groups terminating the surfaces. If required, the true "facet−facet" separation distance may be obtained by adding 2× the C−H or C−OH bond lengths.

In the case of the C_{705} ND, six different types of interaction configurations are examined including the (100)|(100), (100)|(110), (100)|(111), (110)|(110), (110)|(111), and (111)|(111) interacting configurations for the H−C_{705} and OH−C_{705}) NDs. Similarly, the (100)|(100), (100)|(111), (100)|(111)*, (111)|(111), (111)|(111)*, and (111)*|(111)* interaction configurations are considered for the H−C_{837} and OH−C_{837} NDs.

Given the difference in the interacting area of each configuration, total energies calculated are averaged on the arithmetic mean of the area of two interacting facets in each configuration. The areas of the repetitive unit cell for the (100), (111), and (110) surfaces are a_0^2, $(\sqrt{3}/4)a_0^2$, and $(\sqrt{2}/2)a_0^2$, respectively. Here a_0 is the lattice constant of bulk diamond, and the experimental value of 3.567 Å was used. According to the number of the repetitive unit cell on each type of facet in the NDs, the calculated areas of the {100}, {110}, and {111} surfaces of the C_{705} ND are approximately 76.33 Å^2, 26.99 Å^2, and 60.60 Å^2, respectively. Likewise, the calculated areas of the {100} and {111} surfaces of the C_{837} ND are approximately 76.33 Å^2 and 101.91 Å^2, respectively.

The results of the interparticle interactions for the H−C_{705} and H−C_{837} NDs are presented in Figure 2. It was found that all of the interaction configurations considered for the H−C_{705} and H−C_{837} NDs are thermodynamically favorable at their energy minimums, which is distinct from the previous observation in bucky-diamonds.[17] In the H−C_{705} ND, the (110)|(110), (110)|(111), and (111)|(111) configurations have nearly similar exothermic energy minimums (i.e., about −0.223 kJ/(mol·Å^2), −0.221 kJ/(mol·Å^2), and −0.228 kJ/(mol·Å^2) at about 1.99 Å, 1.83 Å, and 1.73 Å, respectively). On the other hand, the (100)|(100), (100)|(110), and (100)|(111) configurations have smaller energy minimums, which are about −0.109 kJ/(mol·Å^2), −0.159 kJ/(mol·Å^2), and −0.151 kJ/(mol·Å^2) at the equilibrium separation distances of 1.97 Å, 1.92 Å, and 1.93 Å, respectively. In the H−C_{837} ND, the (111)|(111)*, (111)|(111), and (111)*|(111)* interaction configurations display relatively larger energy minimums of −0.223 kJ/(mol·Å^2), −0.221 kJ/(mol·Å^2), and −0.228 kJ/(mol·Å^2) at the equilibrium separation distances of 1.99 Å, 1.83 Å, and 1.73 Å, respectively. The (100)|(100), (100)|(110), and (100)|(111) interaction configurations have much smaller energy minimums of −0.109 kJ/(mol·Å^2), −0.159 kJ/(mol·Å^2), and −0.151 kJ/(mol·Å^2) at their equilibrium separation distances of 1.97 Å, 1.92 Å, and 1.93 Å, respectively.

In comparison, the two strongest interactions of bucky-diamonds are −3.106 kJ/(mol·Å^2) and −3.110 kJ/(mol·Å^2) (for the $(111)^-|(111)^0$ and $(100)|(111)^0$ interfaces, respectively).[17] This finding demonstrates that hydrogen functionalization dramatically reduced the interparticle interactions by decreasing the SEP of the unsaturated bucky-diamonds, which supports the use of hydrogenation for the separation of ND aggregates, as proposed by Williams et al.[12]

Although hydrogen termination has been demonstrated to be able to reduce the interparticle interactions in our model NDs, not all the surface functionalization will behave this way. As shown in Figure 3, in the OH−C_{705} ND, the (110)|(110)

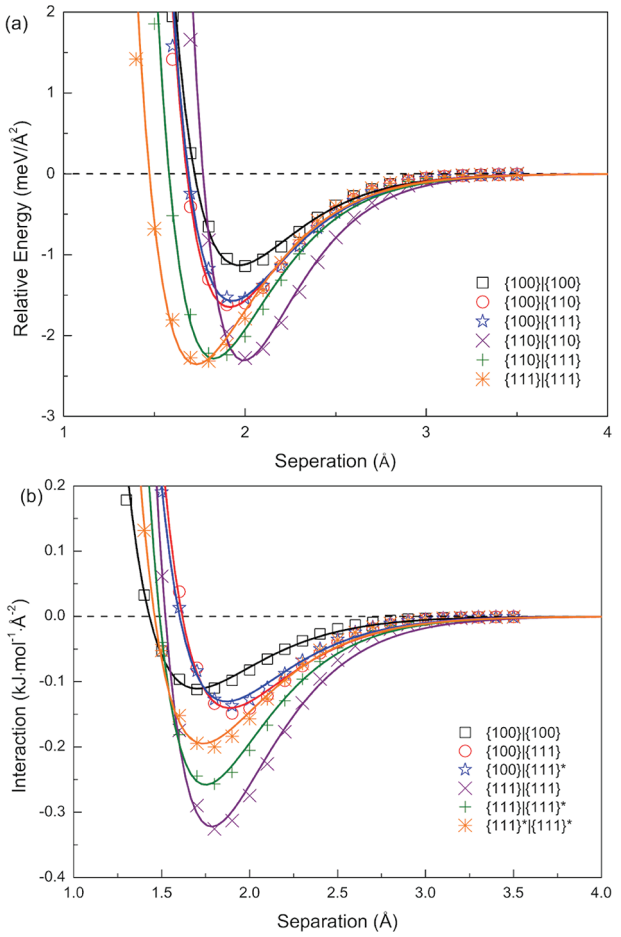

Figure 2. Interparticle interactions as a function of separation distance between two (a) H−C_{705} and (b) H−C_{837} NDs. Calculations are performed at increasing particle/particle separations until further increase of the separation does not noticeably change the interaction between NDs.

interaction has the largest exothermic energy minimum of −1.265 kJ/(mol·Å^2) at a equilibrium separation distance of 1.46 Å, followed by the (110)|(111) and (100)|(110) configurations, whose energy minimums are −0.581 kJ/(mol·Å^2) and −0.574 kJ/(mol·Å^2) at equilibrium separation distances of 1.73 Å and 1.63 Å, respectively. These are much shorter-ranged interactions than the H-terminated particles, but readers are reminded that these distances are between the terminal groups of each participating facet, and that OH−HO interactions are different from H−H interactions. In general, we also see a significant reduction in the strength of the interaction compared with bare bucky-diamonds.

While a reduction in the strength of the interaction upon functionalization with polar groups is counterintuitive, readers are reminded that this is due to the unusually strong electrostatic interaction interaction between bare bucky-diamonds, and that these functionalized surfaces interact in a more typical fashion. The energy minimums of other configurations are −0.259 kJ/(mol·Å^2), −0.316 kJ/(mol·Å^2), and −0.282 kJ/(mol·Å^2) for the (100)|(100), (100)|(111), and (111)|(111) interaction configurations, at the equilibrium separation distances of 1.74 Å, 1.88 Å and 1.99 Å, respectively. These results show that the (110) surfaces are more active than the (100) and (111) surfaces, even though this surface has a lower in-plane atomic density. In the OH−C_{837}, the (100)|

dx.doi.org/10.1021/jz300066j | J. Phys. Chem. Lett. 2012, 3, 896−901

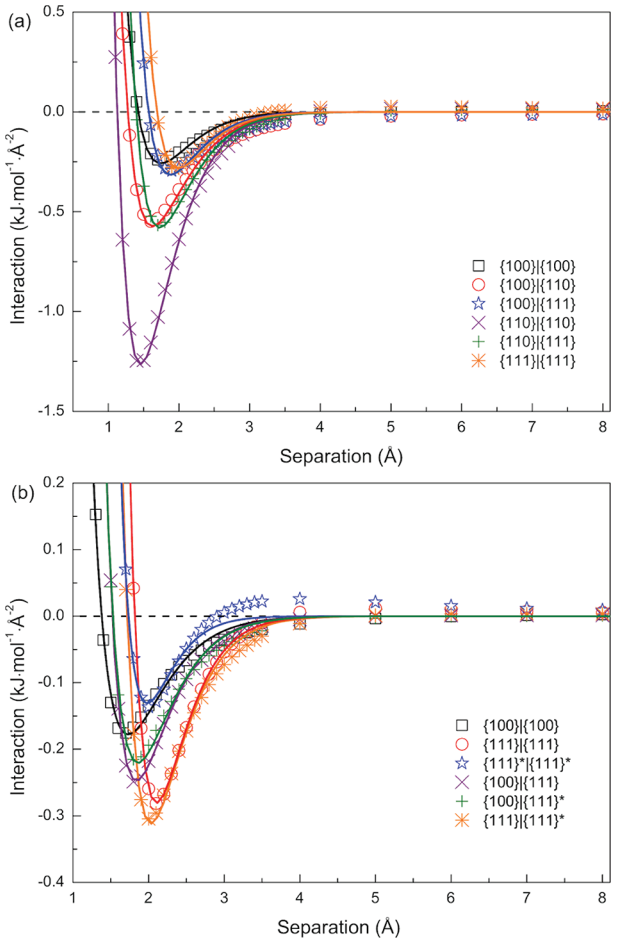

Figure 3. Interparticle interaction as a function of separation distance between two (a) OH−C_{705} and (b) OH−C_{837} NDs. Calculations are performed at increasing particle/particle separations until further increase of the separation does not noticeably change the interaction between NDs.

(100), (100)|(111), (100)|(111)*, (111)|(111), (111)|(111)*, and (111)*|(111)* interaction configurations have exothermic energy minimums of −0.178 kJ/(mol·Å^2), −0.248 kJ/(mol·Å^2), −0.221 kJ/(mol·Å^2), −0.281 kJ/(mol·Å^2), −0.312 kJ/(mol·Å^2), and −0.130 kJ/(mol·Å^2) at the equilibrium separation distances of 1.73 Å, 1.84 Å, 1.86 Å, 2.10 Å, 2.03 Å, and 1.98 Å, respectively. These interactions are longer ranged, akin to H-terminated NDs or "bare" bucky-diamonds.

Readers will also note that some interaction energies are positive, indicating mild repulsion. Although it might initially seem that these are simple interfaces to study, we find that there are more subtle complexities that give rise to these long ranged weak interactions. These facet|facet interactions are not merely intermolecular, as there are a large number of atoms (with different densities and configurations) occupying the interaction radius. Some of these atoms give rise to attraction, and other repulsion, and as the separation increases, the number and type of atoms (and hence their electron clouds) participating in the interaction changes. While this feature is present in all cases to some degree, and is seen in other hydroxylated surfaces,[31] it is most prevalent in ND combinations where the edge|edge interaction is maximized. This issue, however, does not significantly affect the results and conclusions of this study, because the position of the potential energy well does not change, while its depth is only slightly increased.

It is also noted that there are significant differences in the interparticle interactions between the C_{705} and C_{837} NDs. The reason is attributed to the difference in morphology, as the C_{705} has {110} surfaces while the C_{837} does not. These are distinctly different morphologies, with a different number and type of corners and edges, as well as facets. Without these differences, one can expect that the results for the identical interaction configurations of the two NDs (being of similar size) would be similar.

In order to use these findings to generate predictions of the probabilities of different interfaces being present in a real sample, it is important to use a consistent and quantitative way of characterizing the interparticle configurations. Therefore, the relative total energies of two nanoparticles calculated at a given separation distance (with respect to the total energy at $d = \infty$), $E(d)$, were fitted with the universal binding energy relation (UBER):[32]

$$E(d) = -E_0\left(1 + \frac{d - d_0}{l}\right)\exp\left(-\frac{d - d_0}{l}\right) \quad (1)$$

The three fitting parameters (E_0, d_0, l) in this equation represent the energy minimum at the equilibrium separation distance, the equilibrium separation distance, and a scaling length, respectively. The value ($d_0 + l$) indicates the separation distance where the maximum force is achieved, and is more conveniently defined so that the second derivative of the scaled energy-distance curve is unity at equilibrium. Using the UBER fitting parameters presented in Table 1, we can easily distinguish between long-ranged and short-ranged interactions, and identify the true energy minima.

On the basis of these energy minima, we can also determine the conditional probability (P) of different types of interfaces, irrespective of size. The conditional probability is defined as $P_i = E_i/\sum E_i$, where E_i denotes the interaction energy of configuration i. These results are useful in estimating the probability of observation for different types of self-assembled or random superstructures. We can see from these results that interactions involving {110} facets have a significantly greater probability than those that do not. It is also interesting to note the (100)|(111) interaction configuration in both NDs, which have opposite electrostatic potential, is not the most energetically favorable. This is consistent with observation of bucky-diamonds (where a neutral facet was always present in each stable interface), but is inconsistent with the fact that the incoherence of the interface arising from the graphitization and "bubbling" of the (111) facet is eliminated in the presence of functional groups. This suggests that in addition to the Coulombic interactions, hydrogen bonding between surface hydroxyl groups is also involved in the interparticle interaction, especially on the {110} surfaces. This type of weak bonding comes into play because the anisotropy in the SEP (and hence the Coulombic interaction) have been quelled. In general, since real specimens contain a large number of isolated NDs with disperse sizes and shapes, until a reasonable experimental estimate of the polydispersivity of ND, and the local order and density of aggregates is known, an estimate of the "strength" of the ND aggregates and agglutinates remains elusive.

These findings provide a basis for the evaluation of aggregation of realistic diamond nanoparticles of any size assuming that these particles are similar in morphology to our

dx.doi.org/10.1021/jz300066j | J. Phys. Chem. Lett. 2012, 3, 896−901

Table 1. UBER Fitting Parameters of Interaction Configurations, as Well as Corresponding Conditional Probabilities for Hydrogen- and Hydroxyl-Terminated C_{705} and C_{837} NDs

NDs	interface	ΔE_0 (kJ·mol^{-1}·Å^{-2})	d_0 (Å)	l (Å)	P (%)
H−C_{705}	(100)|(100)	0.109	1.967	0.246	8.2
	(100)|(110)	0.159	1.916	0.237	18.0
	(100)|(111)	0.151	1.930	0.242	9.0
	(110)|(110)	0.223	1.993	0.226	33.5
	(110)|(111)	0.221	1.827	0.247	21.4
	(111)|(111)	0.228	1.731	0.258	9.9
H−C_{837}	(100)|(100)	0.111	1.703	0.273	3.3
	(100)|(111)	0.141	1.886	0.269	9.2
	(100)|(111)*	0.130	1.869	0.267	8.6
	(111)|(111)	0.322	1.784	0.263	32.8
	(111)|(111)*	0.258	1.750	0.262	26.2
	(111)*|(111)*	0.195	1.736	0.276	19.9
OH−C_{705}	(100)|(100)	0.259	1.743	0.322	5.4
	(100)|(110)	0.574	1.625	0.349	17.9
	(100)|(111)	0.316	1.877	0.308	5.2
	(110)|(110)	1.265	1.457	0.331	52.6
	(110)|(111)	0.581	1.726	0.332	15.6
	(111)|(111)	0.282	1.993	0.305	3.4
OH−C_{837}	(100)|(100)	0.178	1.731	0.350	4.8
	(100)|(111)	0.248	1.837	0.317	14.8
	(100)|(111)*	0.221	1.856	0.329	13.2
	(111)|(111)	0.281	2.103	0.288	26.1
	(111)|(111)*	0.312	2.030	0.314	29.0
	(111)*|(111)*	0.130	1.982	0.246	12.1

models (i.e., are terminated by combinations of {100}, {110} and {111} facets). We find that the interparticle interaction between functionalized NDs is weaker than that between "bare" bucky-diamond, and the functionalized NDs exhibit some tendency toward self-assembly if sufficient {110} facets are present. However, with the absence of the {110} facets, the conditional probabilities of different interactions are very similar, and random aggregates are likely to form. While this provides some opportunity to engineer different types of aggregates, superstructures of functionalized NDs will be fragile, and will be easily perturbed below the characteristic desorption temperatures of the surface groups under different conditions. Functionalization is very important in moderating the interaction of NDs with other entities (such as drugs), but this comes at the cost of largely eliminating the strong CICI interactions that are characteristic of bare bucky-diamonds.

Future work will be directed toward understanding the functionalization of the NDs, and the nature and strength of the particle−particle interactions under charged conditions. The attractive and repulsive electrostatic forces described here may be affected by deprotonation (positive) or dehydroxylation (negative) of the surface functional groups, just as they are when bare bucky-diamonds are anionic.[18]

AUTHOR INFORMATION

Corresponding Author

*E-mail: amanda.barnard@csiro.au.

Notes

The authors declare no competing financial interest.

ACKNOWLEDGMENTS

Computational resources for this project have been supplied by the National Computing Infrastructure (NCI) national facility under MAS Grant q27.

REFERENCES

(1) Achatz, P.; Garrido, J. A.; Williams, O. A.; Bruno, P.; Gruen, D. M.; Kromka, A.; Steinmüller, D.; Stutzmann, M. Structural, Optical, and Electronic Properties of Nanocrystalline and Ultrananocrystalline Diamond Thin Films. *Phys. Status Solidi A* **2007**, *204*, 2874.

(2) Hu, Y. H.; Shenderova, O. A.; Hu, Z.; Padgett, C. W.; Brenner, D. W. Nanostructures for Advanced Composites. *Rep. Prog. Phys.* **2006**, *69*, 1847.

(3) Chao, J.-I.; Perevedentseva, E.; Chung, P.-H.; Liu, K.-K.; Cheng, C.-Y.; Chang, C.-C.; Cheng, C.-L. Nanometer-Sized Diamond Particle as a Probe for Biolabeling. *Biophys. J.* **2007**, *93*, 2199.

(4) *Nanodiamonds: Applications in Biology and Nanoscale Medicine*; Ho, D., Ed.; Springer Science + Business Media: New York, 2009.

(5) Zhang, X.-Q.; Chen, M.; Lam, R.; Xu, X.; Ōsawa, E.; Ho, D. Polymer-Functionalized Nanodiamond Platforms as Vehicles for Gene Delivery. *ACS Nano* **2009**, *3*, 2609−2616.

(6) Schrand, A. M.; Hens, S. A. C.; Shenderova, O. A. Nanodiamond Particles: Properties and Perspectives for Bioapplications. *Crit. Rev. Solid State Mater. Sci.* **2009**, *34*, 18.

(7) Chen, M.; Pierstorff, E. D.; Lam, R.; Li, S. Y.; Huang, H.; Osawa, E.; Ho, D. Nanodiamond-Mediated Delivery of Water-Insoluble Therapeutics. *ACS Nano* **2009**, *3*, 2016−2022.

(8) Barnard, A. S. Diamond Standard in Diagnostics: Nanodiamond Biolabels Make Their Mark. *Analyst* **2009**, *134*, 1751−1764.

(9) Ōsawa, E. Recent Progress and Perspectives in Single-Digit Nanodiamond. *Diamond Relat. Mater.* **2007**, *16*, 2018−2022.

(10) Huang, H.; Pierstorff, E.; Ōsawa, E.; Ho, D. *Nano Lett.* **2007**, *7*, 3305−3314.

(11) Kruger, A.; Kataoka, F.; Ozawa, M.; Fujino, T.; Suzuki, Y.; Aleksenskii, A. E.; VulŠ, A. Y.; Ōsawa, E. Unusually Tight Aggregation in Detonation Diamond: Identification and Disintegration. *Carbon* **2005**, *43*, 1722−1730.

(12) Williams, O. A.; Hees, J.; Dieker, C.; Jager, W.; Kirste, L.; Nebel, C. E. Size-Dependent Reactivity of Diamond Nanoparticles. *ACS Nano* **2010**, *4*, 4824−4830.

(13) Xu, K.; Xue, Q. J. A New Method for Deaggregation of Nanodiamond from Explosive Detonation: Graphitization−Oxidation Method. *Phys. Solid State* **2004**, *46*, 649−650.

(14) Osswald, S.; Yushin, G.; Mochalin, V.; Kucheyev, S. O.; Gogotsi, Y. Control of sp^2/sp^3 Carbon Ratio and Surface Chemistry of Nanodiamond Powders by Selective Oxidation in Air. *J. Am. Chem. Soc.* **2006**, *128*, 11635−11642.

(15) Huang, H.; Dai, L.; Wang, D. H.; Tan, L.-S.; Ōsawa, E. Large-Scale Self-Assembly of Dispersed Nanodiamonds. *J. Mater. Chem.* **2008**, *18*, 1347−1352.

(16) Barnard, A. S.; Sternberg, M. Crystallinity and Surface Electrostatics in Diamond Nanoparticles. *J. Mater. Chem.* **2007**, *17*, 4811.

(17) Barnard, A. S. Self-Assembly in Nanodiamond Agglutinates. *J. Mater. Chem.* **2008**, *18*, 4038.

(18) Chang, L.-Y.; Ōsawa, E.; Barnard, A. S. Confirmation of the Electrostatic Self-Assembly of Nanodiamonds. *Nanoscale* **2011**, *3*, 958−962.

(19) Hees, J.; Kriele, A.; Williams, O. A. Electrostatic Self Assembly of Diamond Nanoparticles. *Chem. Phys. Lett.* **2011**, *509*, 12−15.

(20) *Ultrananocrystalline Diamond: Synthesis, Properties and Applications*; Shenderova, O. A., Gruen, D. M., Eds.; William Andrew Publishing: Norwich, NY, 2006.

(21) Lai, L.; Barnard, A. S. Stability of Nanodiamond Exposed to N, NH and NH_2. *J. Phys. Chem. C* **2011**, *115*, 6218−6228.

(22) Lai, L.; Barnard, A. S. Modeling the Atomic Structure and Thermostability of Oxygen, Hydroxyl, and Water Functionalization of Nanodiamonds. *Nanoscale* **2011**, *3*, 2566−2575.

(23) Porezag, D.; Frauenheim, T.; Köhler, T.; Seifert, G.; Kaschner, R. Construction of Tight-Binding-like Potentials on the Basis of Density-Functional Theory: Application to Carbon. *Phys. Rev. B* **1995**, *51*, 12947−12957.
(24) Frauenheim, T.; Seifert, G.; Elstner, M.; Niehaus, T.; Köhler, C.; Amkreutz, M.; Sternberg, M.; Hajnal, Z.; Carlo, A. D.; Suhai, S. Atomistic Simulations of Complex Materials: Ground-State and Excited-State Properties. *J. Phys.: Condens. Matter* **2002**, *14*, 3015.
(25) Barnard, A. S.; Sternberg, M. Substitutional Nitrogen in Nanodiamond and Bucky-Diamond Particles. *J. Phys. Chem. B* **2005**, *109*, 17107.
(26) Bradac, C.; Gaebel, T.; Naidoo, N.; Rabeau, J. R.; Barnard, A. S. Prediction and Measurement of the Size-Dependent Stability of Fluorescence in Diamond over the Entire Nanoscale. *Nano Lett.* **2009**, *9*, 3555−3564.
(27) Bradac, C.; Gaebel, T.; Naidoo, N. N.; Sellars, M. J.; Twamley, J.; Brown, L.; Barnard, A. S.; Plakhotnik, T.; Zvyagin, A. V.; Rabeau, J. R. Observation and Control of Blinking Nitrogen Vacancy Centres in Discrete Nanodiamonds. *Nat. Nanotechnol.* **2010**, *5*, 345−349.
(28) Kohler, C.; Frauenheim, T. Molecular Dynamics Simulations of CF_x (x = 2,3) Molecules at Si_3N_4 and SiO_2 Surfaces. *Surf. Sci.* **2006**, *600*, 453−460.
(29) Ōsawa, E.; Ho, D.; Huang, H.; Korobov, M. V.; Rozhkova, N. N. Consequences of Strong and Diverse Electrostatic Potential Fields on the Surface of Detonation Nanodiamond Particles. *Diamond Relat. Matter* **2009**, *18*, 904−909.
(30) The absolute value of electrostatic potential is not important in this study. What matters is the sign of potential, which indicates whether the interaction between two facets is attractive or repulsive. Because we have not assumed a specific situation (for example, in vacuum or in liquid), the value of dielectric constant used is arbitrary. If it was set to be 1.0, one can expect the value in the legend would be multiplied by 10. This does not change the nature of interactions, only the scale in Figure 1.
(31) Wright, L. B.; Walsh, T. R. Facet Selectivity of Binding on Quartz Surfaces: Free Energy Calculations of Amino-Acid Analogue Adsorption. *J. Phys. Chem. C* **2012**, *116*, 2933−2945.
(32) Banerjea, A.; Smith, J. R. Origins of the Universal Binding-Energy Relation. *Phys. Rev. B* **1988**, *37*, 6632.